Article

Discovery Medicine 2026; 38(211): 2524–2534
https://doi.org/10.24976/Discov.Med.202638211.199

A Bridge From the Gut: Azithromycin Links to AMPK/SIRT1 Activation, Rectifies Th17/Treg Balance and Alleviates COPD Associated With Gut Microbiota-TMAO Modulation

Changqing Xu[1,†], Guoping Jiang[2,*,†], Guohu Zhang[3], Jiang Wu[4], Weiguo Rao[4], Songtao Jiang[4], Lanjuan Zhang[4], Lu Zhang[4], Yuezhong Shen[1], Liquan Hong[3]

[1]Respiratory Department, The Affiliated Hospital of Hangzhou Normal University, 310000 Hangzhou, Zhejiang, China
[2]Respiratory Department, Deqing County Third People's Hospital, 313201 Huzhou, Zhejiang, China
[3]The Emergency Department, The Affiliated Hospital of Hangzhou Normal University, 310000 Hangzhou, Zhejiang, China
[4]The Emergency Department, The Fourth People's Hospital of Lin'an District, 311321 Hangzhou, Zhejiang, China
*Correspondence: jiangguopingp_JGP@163.com (Guoping Jiang)
[†]These authors contributed equally.
Submitted: 3 February 2026 Revised: 4 June 2026 Accepted: 22 June 2026 Published: 24 August 2026

Background: The intestinal microbial ecosystem has emerged as an important contributor to chronic obstructive pulmonary disease (COPD) pathogenesis. Azithromycin (AZI), a commonly used therapeutic agent for COPD, has antibacterial and anti-inflammatory effects. This study aims to explore the mechanism by which AZI regulates the intestinal microbial ecosystem to ameliorate COPD.

Methods: A rat COPD model was established by cigarette smoke (CS) exposure. The animals were pretreated with AZI (0.5, 5, 50 mg/kg) with or without the adenosine monophosphate-activated protein kinase (AMPK) inhibitor Compound C. Pulmonary dysfunction and colon injury in COPD rats were evaluated by detecting forced expiratory volume within 0.3 seconds (FEV0.3), forced vital capacity (FVC), as well as hematoxylin and eosin staining. Flow cytometry was used to detect T helper 17 (Th17)/regulatory T (Treg) cell balance in colon tissue. Inflammatory factors and secretory IgA (sIgA) levels were detected using quantitative real-time polymerase chain reaction (qRT-PCR) and enzyme-linked immunosorbent assay (ELISA). Trimethylamine N-oxide (TMAO) content was determined by liquid chromatography with triple-quadrupole mass spectrometry. AMPK/sirtuin 1 (SIRT1) pathway-related proteins were detected using Western blotting.

Results: AZI dose-dependently alleviated CS-induced lung dysfunction and colon tissue injury ($p < 0.05$), reduced the ratio of Th17/Treg, facilitated the expression levels of interleukin (IL)-10 and sIgA, and inhibited the levels of pro-inflammatory factors and TMAO ($p < 0.05$). In addition, AZI activated the AMPK pathway and upregulated SIRT1 expression in colon tissues ($p < 0.05$). Critically, the protective effects of AZI were partially reversed by co-treatment with the AMPK inhibitor Compound C ($p < 0.05$).

Conclusion: AZI may regulate the Th17/Treg cell balance in association with TMAO reduction and AMPK/SIRT1 activation, thereby improving intestinal mucosal immunity in COPD rats. These findings highlight the potential of targeting the gut microbiota and mucosal immunity as a therapeutic strategy for COPD management.

Keywords: chronic obstructive pulmonary disease; azithromycin; Treg/Th17 balance; trimethylamine N-oxide; AMPK/SIRT1 pathway

Introduction

Chronic obstructive pulmonary disease (COPD), a respiratory disease that seriously endangers public health, has a high incidence rate and can lead to irreversible decline in lung function [1]. The pathogenesis of COPD is usually associated with long-term exposure to harmful particles or cigarette smoke (CS), which can trigger abnormal inflammation in the airways and alveoli [2]. In addition, with the development of the gut-lung axis concept, the role of intestinal flora in COPD has attracted increasing attention. COPD patients are prone to intestinal inflammation and intestinal cell damage, which may lead to intestinal flora imbalance. This imbalance can promote intestinal flora displacement, and the release of intestinal endotoxins and inflammatory mediators, thereby accelerating the pathological progression of COPD [3]. Gut dysbiosis also promotes the production of trimethylamine N-oxide (TMAO), a key microbiota-derived metabolite that exacerbates systemic and pulmonary inflammation [4]. TMAO can suppress the AMPK/sirtuin 1 (SIRT1) signaling pathway, which plays a key role in regulating cellular senes-

cence and vascular homeostasis [5]. Therefore, preventing COPD by regulating the intestinal microbial ecosystem has become a current research hotspot.

Azithromycin (AZI) is a macrolide antibiotic with anti-inflammatory effects and has good safety and tolerability in stable COPD [6]. Several randomized controlled studies have shown that maintenance treatment with AZI significantly prevents COPD exacerbations [7,8]. AZI mainly inhibits the synthesis of bacterial proteins, thereby exerting antibacterial effects. In addition, AZI also has anti-inflammatory activity. Previous studies have reported that AZI can reduce airway inflammation in patients with allergic asthma by modulating the intestinal microflora [9]. Therefore, AZI may also prevent COPD by regulating the intestinal microbial ecosystem. However, how AZI regulates the intestinal microbial ecosystem needs further investigation.

It is worth noting that T helper 17 (Th17)/regulatory T (Treg) cell balance plays an important role in COPD and intestinal diseases [10,11]. Th17 cells aggravate inflammation by releasing pro-inflammatory factors such as interleukin (IL)-17, thereby promoting COPD progression and intestinal inflammation, whereas Treg cells release anti-inflammatory factors such as IL-10 to suppress inflammatory responses [11]. Studies have shown that during the imbalance of intestinal microflora, due to the excessive growth of pathogenic bacteria and the decrease in intestinal microflora diversity, the Th17/Treg balance shifts toward Th17 cells, further aggravating inflammatory responses and creating a vicious circle [10]. This dysbiosis-driven Th17/Treg imbalance is closely intertwined with the impaired TMAO-AMPK/SIRT1 axis, collectively exacerbating mucosal inflammation along the gut-lung axis. Therefore, restoring the Th17/Treg cell balance has become a key therapeutic target in COPD. Interestingly, AZI has the ability to regulate Th17 and Treg cells [12]. Accordingly, we speculate that AZI may prevent COPD by regulating the Th17/Treg cell balance and stabilizing the intestinal microbial ecosystem.

Materials and Methods

Animal Experiments and Treatments

Male Sprague–Dawley rats (N = 60) aged 7 weeks (200 ± 20 g) were purchased from Hangzhou Medical College and housed under a 12-hour light/dark cycle with free access to water and food. The protocol was approved by the Ethics Committee of Zhejiang Provincial Laboratory Animal Center for Experimental Animals Welfare (ZJCLA-IACUC-20011009). The animal experiments were conducted in adherence with the ARRIVE Guidelines 2.0.

Rats were randomly divided into six groups, including a control group, a model group, a model+AZI-0.5 group, a model+AZI-5 group, a model+AZI-50 group and a model+AZI-50+Compound C group. Except for the control group, rats in all other groups were exposed to CS as previously described [13]. Briefly, rats were placed in a 1 m^3 whole-body inhalation chamber filled with CS for 1 hour every day for 4 weeks (6 days per week). The cigarette, containing 10 mg tar, 0.8 mg nicotine, and 13 mg carbon monoxide content, was provided by China Tobacco Anhui Industrial Co., Ltd. 20 cigarettes were lit daily in the whole-body inhalation chamber. The rats in the model+AZI groups were intragastrically administered different concentrations of AZI (0.5, 5, 50 mg/kg, HY-17506, MedChemExpress, Monmouth Junction, NJ, USA) 1 hour before the CS exposure every day. Rats in the model+AZI (50 mg/kg)+Compound C group were additionally administered Compound C (5 mg/kg, i.v. [14]; HY-13418A, MedChemExpress, Monmouth Junction, NJ, USA) 30 minutes before the CS exposure to inhibit AMPK signaling. At the end of the experiment, all animals were deeply anesthetized by an intraperitoneal injection of 2% pentobarbital sodium (100 mg/kg) and then euthanized by cervical dislocation. Investigators were blinded to group allocation during all subsequent experimental procedures, including pulmonary function measurements, hematoxylin and eosin (H&E) staining image acquisition and analysis, flow cytometry, quantitative real-time polymerase chain reaction (qRT-PCR), enzyme-linked immunosorbent assay (ELISA), LC-MS/MS, Western blotting, and statistical analysis. Rats were randomly divided into six groups (n = 10 per group). For H&E staining, three rats were randomly selected from each group. For all other molecular assays (flow cytometry, qRT-PCR, ELISA, LC-MS/MS, and Western blot), three rats were randomly selected from each group, and all experiments were performed in triplicate as technical replicates.

Pulmonary Function Measurement

After anesthesia with 2% pentobarbital sodium (45 mg/kg), rats were connected to a pulmonary function testing system (PFT-MR, Tarzan-tech, Changsha, China) through tracheal intubation. Mechanical ventilation was applied during the measurement to avoid anesthesia-related respiratory depression. Before data acquisition, the system was stabilized, and ventilation parameters were set as follows: respiratory frequency = 65 breaths/min, tidal volume = 8 mL/kg, and inspiratory to expiratory ratio = 1:2. For each animal, three consecutive stable measurements were recorded, and the average values were used for analysis. FEV 0.3 (forced expiratory volume within 0.3 seconds), FVC (forced vital capacity), and (FEV 0.3/FVC)% were automatically analyzed to evaluate the degree of airway obstruction and verify the successful establishment of the pulmonary obstruction model [15,16].

H&E Staining

After detecting lung function, rats were deeply anesthetized with an intraperitoneal injection of 2% pentobarbital sodium (100 mg/kg), then euthanized by cervical dislo-

cation, and their lung and colon tissues were collected and fixed in 4% paraformaldehyde (TW26423, TW-reagent, Shanghai, China). Tissue was embedded in paraffin and cut into 4-μm slices, then dewaxed in xylene and soaked in gradient ethanol. After the slices were processed, the hematoxylin solution and eosin solution in the H&E kit (GF11014, Glpbio, Beijing, China) were applied dropwise to the slices, respectively. The slices were then routinely dehydrated, cleared and mounted. For each group, tissues from three rats were examined. From each tissue sample, three non-serial sections were prepared, and five non-overlapping fields per section were randomly selected for image acquisition. Finally, the histological changes were observed under a microscope (KD-810A, KDYXBIO, Jinhua, China) to further confirm the successful establishment of the pulmonary obstruction model [17]. All image acquisitions were performed using standardized procedures, and the operator was blinded to group allocation.

Flow Cytometry

First, the colon tissue was cut into small pieces and incubated in RPMI-1640 culture medium (R101, YaJi Biological, Shanghai, China) containing type III collagenase (TBD20180071, TBD science, Tianjin, China). After filtration, rat lymphocytes were enriched using a rat organ tissue lymphocyte isolation kit (LTS1083P, TBD science, Tianjin, China). The cells were then fixed, permeabilized and stained with a cocktail of fluorescent antibodies, including PE anti-rat IL-17A (12-7177-81, ThermoFisher, Waltham, MA, USA), Alexa Fluor® 647 anti-rat Foxp3 (320014, Biolegend, USA), FITC anti-rat CD4 (201505, Biolegend, San Diego, CA, USA), and Alexa Fluor 750 anti-rat CD25 (NB100-64761-AF750, Novusbio, Centennial, CO, USA). For intracellular IL-17A staining, the isolated lymphocytes were stimulated with eBioscience™ Cell Stimulation Cocktail (cat# 00-4975-93, ThermoFisher, Waltham, MA, USA) at 37 °C for 4–6 hours. The results were analyzed using flow cytometry (Epics XL-II, Beckman, Brea, CA, USA). The gating strategy was applied as follows: first, lymphocytes were gated based on FSC/SSC; then, doublets were excluded using FSC-A vs. FSC-H; dead cells were excluded by staining with a fixable viability dye (cat# 423105, Zombie NIR™, BioLegend, San Diego, CA, USA) prior to surface staining; subsequently, $CD4^+$ T cells were pregated. Within the $CD4^+$ population, Treg cells were identified as $CD25^+Foxp3^+$ and Th17 cells as IL-$17A^+$. For quality control, single-color compensation controls were prepared using UltraComp eBeads (Invitrogen, Waltham, MA, USA) stained with each antibody individually, and spectral overlap was automatically corrected by the flow cytometer software. Fluorescence-minus-one (FMO) controls were used for each fluorochrome (FITC, PE, Alexa Fluor 647, and Alexa Fluor 750) to define the positivity thresholds and set accurate gates. Dead cells were excluded using the viability dye as described above.

qRT-PCR

Using the reverse transcription kit (NN01012, NucleoTech, Beijing, China), the RNA isolated by TRIzol (AN51L758, Life-iLab, Shanghai, China) was reverse-transcribed into cDNA. Fluorescence detection was carried out using the SYBR Green kit (AN19L918, Life-iLab, Shanghai, China). The cycling conditions were as follows: initial denaturation at 95 °C for 10 minutes, followed by 40 cycles of denaturation at 95 °C for 15 seconds, annealing at 60 °C for 30 seconds, and extension at 72 °C for 30 seconds. A melting curve analysis was performed from 60 °C to 95 °C to verify amplicon specificity. The expression of the target genes was normalized to that of glyceraldehyde-3-phosphate dehydrogenase (GAPDH) using the $2^{-\Delta\Delta CT}$ method. The stability of GAPDH as an internal control was validated across all experimental groups; the coefficient of variation (CV) of GAPDH Ct values was <5%, and no significant differences in GAPDH expression were observed among groups ($p > 0.05$).

A standard curve was generated using serial dilutions of cDNA to determine primer efficiency. The amplification efficiency for each primer pair ranged from 95% to 105%. All reactions were performed in technical triplicate. The qRT-PCR primer sequences are listed in Table 1.

Table 1. Primers used in this study.

Primer name	5′ to 3′
TNF-α (Rat) Forward	GGCTTTCGGAACTCACTGGA
TNF-α (Rat) Reverse	CCCGTAGGGCGATTACAGTC
IL-1β (Rat) Forward	TTGAGTCTGCACAGTTCCCC
IL-1β (Rat) Reverse	GTCCTGGGGAAGGCATTAGG
IL-6 (Rat) Forward	CACTTCACAAGTCGGAGGCT
IL-6 (Rat) Reverse	AGCACACTAGGTTTGCCGAG
IL-10 (Rat) Forward	CATTCCATCCGGGGTGACAA
IL-10 (Rat) Reverse	GTAGATGCCGGGTGGTTCAA
IL-17 (Rat) Forward	GTGAAGGCAGCGGTACTCAT
IL-17 (Rat) Reverse	ATGTGGTGGTCCAACTTCCC
GAPDH (Rat) Forward	AGGAAATGATGACCTCCTGAACT
GAPDH (Rat) Reverse	GAAGATGCGGTCACCTCACA

Abbreviation: GAPDH, Glyceraldehyde-3-phosphate dehydrogenase; TNF-α, tumor necrosis factor-α; IL, interleukin.

ELISA

The secretory IgA (sIgA) content in jejunum and ileum tissues was determined using an ELISA kit (TW2221, TW-reagent, Shanghai, China). Briefly, the tissue homogenate was centrifuged at 1000 ×g for 15 minutes to collect the supernatant. The supernatant and standards were added to the plate. Then, the antibody labeled with horseradish peroxidase was added to each well and incubated for 1 hour. Thereafter, the substrate A, substrate B and the termination solution were added to the plate in turn.

The OD value at 450 nm was detected under a microreader (BK-9622, LBMED, Guangzhou, China). The sIgA concentration in each sample was calculated from a standard curve and then normalized to the total protein concentration of the corresponding tissue homogenate, as determined by the BCA method. Results are expressed as ng of sIgA per mg of total protein.

The standard curve was generated using serial dilutions of the provided sIgA standard (range: 0.156–20 ng/mL). The standard curve showed a four-parameter logistic (4-PL) fit with R^2 >0.99. All samples were measured in duplicate, and Inter-assay precision was assessed by running quality control samples in three independent experiments.

Liquid Chromatography With Triple-Quadrupole Mass Spectrometry

Trimethylamine N-oxide (TMAO) levels in plasma were determined using liquid chromatography with triple-quadrupole mass spectrometry as previously described [18]. Briefly, plasma samples (50 µL) were mixed with 150 µL of ice-cold acetonitrile containing the internal standard (TMAO-d9, 1 µM) to precipitate proteins. The mixture was vortexed for 1 min and centrifuged at 14,000 ×g for 10 min at 4 °C. The supernatant (100 µL) was transferred to an autosampler vial for analysis. Separation was performed on an Agilent Poroshell 120 HILIC column, and detected in multiple reaction monitoring (MRM) mode. The injection volume was 5 µL, and the total run time was 6 min.

Calibration was performed using a stable isotope-labeled internal standard (TMAO-d9). The calibration curve was linear over the concentration range of 0.1–50 µmol/L (R^2 >0.999). The lower limit of quantification (LLOQ) was 0.1 µmol/L. Intra- and inter-day precision (relative standard deviation, RSD) were <10%, and accuracy (relative error, RE) ranged from 92% to 108%. The recovery of TMAO ranged from 95% to 102%. The concentration unit was expressed as µmol/L.

Western Blotting

A BCA Protein Assay kit (YWB002, YFXBIO, Shanghai, China) was used to measure the protein concentrations after the total protein was extracted using RIPA Lysis Buffer (AP01L013, Life-iLab, China). Equal amounts of total protein (30 µg per lane) were separated by 10% SDS-PAGE (190916-40, YaJi Biological, Shanghai, China), and then transferred to a PVDF membrane (PVDF, WJ001S, epizyme, Beijing, China). For routine protein detection, the membrane was blocked with 5% non-fat milk in TBST for 1 hour at room temperature. For phosphorylated protein detection, BSA was used instead of non-fat milk to avoid non-specific cross-reactivity with phospho-epitopes present in milk proteins. The blocked membrane was then incubated with primary antibodies and washed three times with TBST.

The membrane was then incubated with horseradish peroxidase (HRP)-conjugated secondary antibodies, and subsequently washed six times. Details of the antibodies used are shown in Table 2.

The imaging tool (GeneTools, SynGene, Frederick, MD, USA, software version 4.3.2) and ECL kit (YWB003, YFXBIO, Shanghai, China) were used to analyze the chemiluminescent signals. p-AMPK levels were normalized to total AMPK (expressed as the p-AMPK/AMPK ratio), and total AMPK and all other target proteins were normalized to β-actin as the loading control. All quantifications were performed using ImageJ software from at least three independent biological replicates.

Statistical Analysis

The experiments were repeated at least three times. All experimental results were analyzed using the SPSS 21.0 system (SPSS Inc., Chicago, IL, USA) and expressed as mean ± SD. Homogeneity of variances was assessed using Levene's test. For comparisons among the experimental groups, one-way ANOVA was performed, followed by Bonferroni's post-hoc test for multiple comparisons. $p < 0.05$ was considered statistically significant.

Results

AZI Alleviated CS-Induced Lung Dysfunction and Colon Tissue Injury

Compared with the control group, the FEV0.3, FVC, and FEV0.3/FVC of the model group rats were significantly reduced (Fig. 1A–C, $p < 0.001$). However, higher FEV0.3, FVC, and FEV0.3/FVC were observed in COPD rats pretreated with different concentrations of AZI compared to the model group (Fig. 1A–C, $p < 0.01$). Notably, the beneficial effects of AZI (50 mg/kg) on these pulmonary function parameters were attenuated by co-administration of the AMPK inhibitor Compound C (Fig. 1A–C, $p < 0.05$). Compared with the model group, higher FEV0.3 and FEV0.3/FVC were observed in the model+AZI+Compound C group (Fig. 1A–C, $p < 0.05$). Next, we performed H&E staining on lung and colon tissues. Model rats' lung tissue showed infiltration of inflammatory cells around the bronchus, thickening of mucosal epithelium, and enlargement of alveoli (Fig. 1D). At the same time, more infiltrating cells, fewer goblet cells, and looser intercellular spaces were observed in the colon tissue of model rats (Fig. 1E). However, these abnormalities were alleviated by AZI in a concentration- dependent manner (Fig. 1D,E). Importantly, the protective effects of AZI at the highest dose (50 mg/kg) were partially counteracted by Compound C, as evidenced by aggravated inflammatory cell infiltration and epithelial thickening in the lungs, and increased inflammatory infiltration, reduced goblet cells, and disrupted intercellular integrity in the colon (Fig. 1D,E).

Table 2. Antibodies used in this study.

Name	Host	Antigen site/Catalog	Molecular weight	Dilution	Conjugate	Manufacturer
p-AMPK	Rabbit	Thr172/ab133448	64 kDa	1/1000		abcam, UK
AMPK	Rabbit	ab32047	63 kDa	1/1000		abcam, UK
SIRT1	Rabbit	ab189494	80 kDa	1/1000		abcam, UK
β-actin	Mouse	ab8226	42 kDa	1/10,000		abcam, UK
Goat anti-rabbit IgG (H+L)	goat	ab205718	—	1/2000	HRP	abcam, UK
Goat anti-mouse IgG (H+L)	goat	ab205719	—	1/2000	HRP	abcam, UK

Abbreviation: SIRT1, sirtuin 1.

AZI Regulated Th17/Treg Balance in COPD Rats

To investigate the effect of AZI on the Th17/Treg ratio, flow cytometry was performed. Compared with normal rats, in the colon tissue of COPD rats, the proportion of Treg cells decreased (Fig. 2A,B, $p < 0.001$), the proportion of Th17 cells increased (Fig. 2A,C, $p < 0.001$), and the Th17/Treg ratio increased (Fig. 2A,D, $p < 0.001$). Treatment with AZI concentration-dependently mitigated these alterations by increasing the Treg cell population, reducing the Th17 cell population, and normalizing the Th17/Treg ratio (Fig. 2A–D, $p < 0.001$). However, the beneficial regulatory effects of AZI (50 mg/kg) on this immune balance were markedly reversed by co-treatment with the AMPK inhibitor Compound C, as evidenced by a significant reduction in Treg cells, an increase in Th17 cells, and a resultant higher Th17/Treg ratio compared to the AZI-50 mg/kg monotherapy group (Fig. 2A–D and S1A, $p < 0.001$). In addition, compared with the model group, the proportion of Treg cells was increased, the proportion of Th17 cells was decreased, and the Th17/Treg ratio was decreased in the model+AZI+Compound C group (Fig. 2A–D, $p < 0.01$).

AZI Exerted Anti-Inflammatory Effects and Protected the Intestinal Mucosal Immune System in COPD Rats

We then investigated whether AZI could improve the CS-induced inflammatory response. As expected, the upregulation of pro-inflammatory factors (TNF-α, IL-1β, IL-6 and IL-17) and downregulation of anti-inflammatory factors (IL-10) caused by CS exposure were reversed by AZI in a concentration-dependent manner (Fig. 3A–E, $p < 0.001$). Notably, this anti-inflammatory effect of AZI (50 mg/kg) was attenuated by the co-administration of Compound C, which significantly increased the levels of TNF-α, IL-1β, IL-6, and IL-17, while suppressing IL-10 expression compared to the AZI-50 mg/kg group (Fig. 3A–E, $p < 0.001$). Compared with the model group, IL-1β levels were decreased in the model+AZI+Compound C group (Fig. 3B, $p < 0.01$). In addition, the levels of sIgA in the intestinal mucosa of COPD rats were analyzed by ELISA, and the results showed that the sIgA levels in the model group were lower than those in the control group, while the sIgA levels in the model rats treated with AZI were higher than those in the model group (Fig. 3F, $p < 0.001$). However, the promotion of sIgA by AZI (50 mg/kg) was compromised by the addition of Compound C, leading to lower sIgA concentrations in the jejunum and ileum (Fig. 3F, $p < 0.001$). Furthermore, the level of the gut microbiota metabolite TMAO was also increased in the model group, but was reduced by AZI in a concentration-dependent manner (Fig. 3G, $p < 0.001$). Importantly, the AMPK inhibitor Compound C counteracted the effect of AZI (50 mg/kg), resulting in a marked increase in serum TMAO levels (Fig. 3G, $p < 0.001$).

AZI Modulated the AMPK Pathway and Upregulated SIRT1 Expression in the Colon Tissues of COPD Rats

Western blotting revealed the effects of AZI on the AMPK pathway and SIRT1 expression. The p-AMPK/AMPK ratio in the colon tissue of COPD rats decreased, accompanied by the downregulation of SIRT1 (Fig. 4A–C, $p < 0.001$). Treatment with AZI at 5 mg/kg significantly upregulated SIRT1 expression ($p < 0.05$), but did not significantly affect the p-AMPK/AMPK ratio. AZI at 50 mg/kg significantly increased both the p-AMPK/AMPK ratio and SIRT1 expression(Fig. 4A–C, $p < 0.01$), while the 0.5 mg/kg dose showed no significant effects. Notably, the co-administration of the AMPK inhibitor Compound C with AZI (50 mg/kg) partially reversed this activating effect, resulting in a significant reduction in both the p-AMPK/AMPK ratio and SIRT1 levels compared to the AZI (50 mg/kg) monotherapy group (Fig. 4A–C, $p < 0.01$).

Discussion

We first evaluated the effects of AZI on lung function and colon tissue in COPD rats. FEV0.3 and FVC are commonly used indicators of lung function [19]. It has long been proven that CS induction can lead to a decrease in FEV0.3/FVC [20]. In our study, AZI reversed the decrease in FEV0.3/FVC induced by CS, which is consistent with previously reported results that AZI increases the FEV0.3/FVC ratio in COPD rats [21]. In previous studies, AZI had obvious therapeutic effects on colon injury and lung injury caused by inflammation [22,23]. Consistently, H&E staining in our study showed that AZI improved CS-induced lung tissue and colon tissue injury. Importantly, co-treatment with the AMPK inhibitor Compound C partially attenuated the protective effects of AZI on both lung function and tissue histopathology, underscoring the involvement of AMPK signaling in AZI-mediated protection.

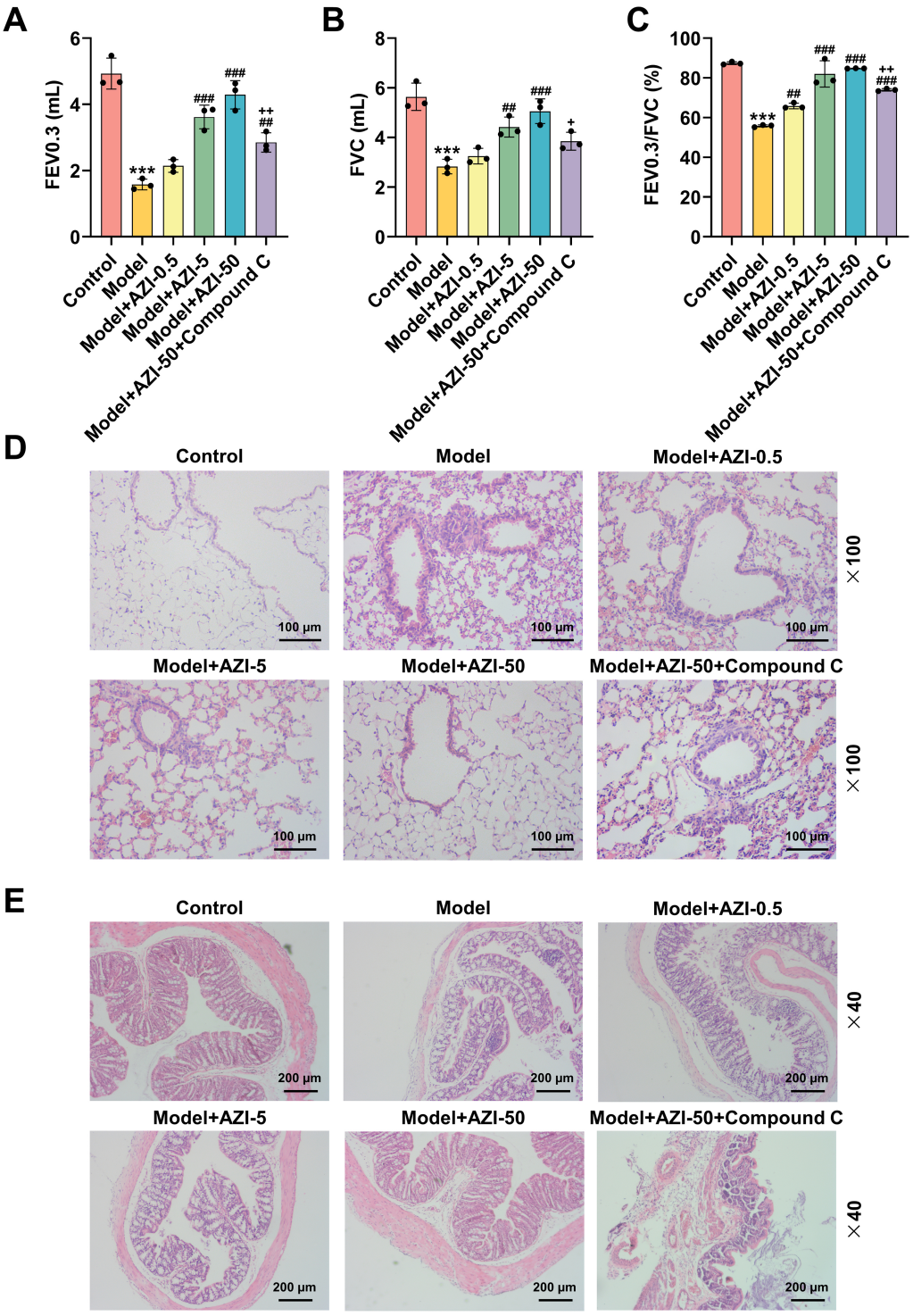

Fig. 1. The effects of AZI on pulmonary function and pathological changes of lung and colon tissue in COPD rats. Rats were pretreated with AZI (0.5, 5, or 50 mg/kg), or AZI (50 mg/kg) plus the AMPK inhibitor Compound C, respectively, and subsequently exposed to cigarette smoke to induce COPD. (A–C) Pulmonary function showing FEV0.3, FVC and (FEV 0.3/FVC) % in all groups. (D) Lung pathological slides by H&E staining (100×, 100 μm). (E) H&E detection of pathological changes of colon tissue (40×, 200 μm). $^{***}p < 0.001$ vs. Control. $^{\#\#}p < 0.01$, $^{\#\#\#}p < 0.001$ vs. Model. $^{+}p < 0.05$, $^{++}p < 0.01$ vs. Model+AZI-50. Data are presented as mean ± SD, and were analyzed using two-way ANOVA followed by Bonferroni's post-hoc test (n = 3 rats per group). AZI, Azithromycin; COPD, chronic obstructive pulmonary disease; FEV 0.3, Forced expiratory volume in 0.3 s; FVC, Forced vital capacity; H&E, hematoxylin and eosin.

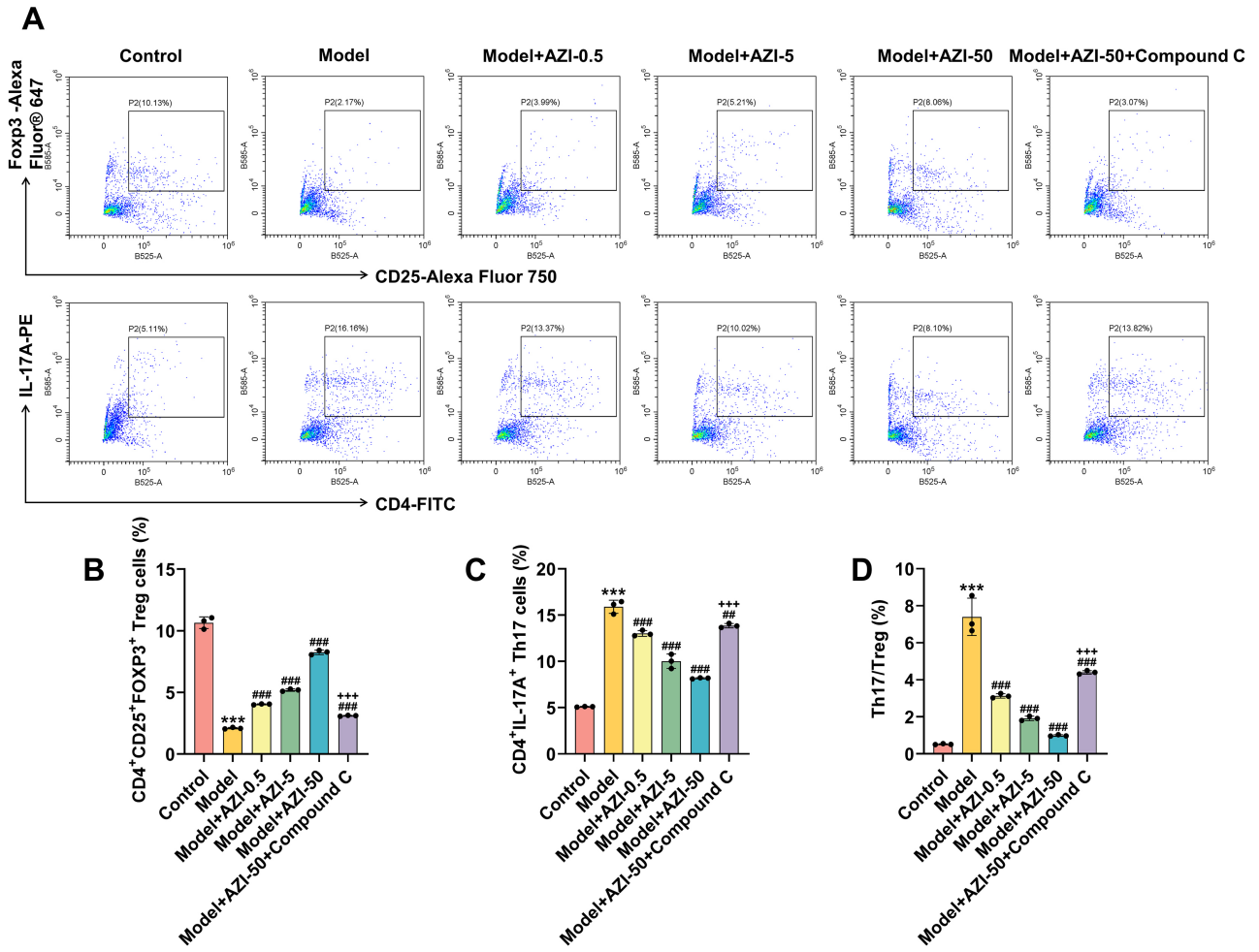

Fig. 2. AZI regulates the Th17/Treg ratio in the colon of COPD rats. Rats were pretreated with AZI (0.5, 5, or 50 mg/kg), or AZI (50 mg/kg) plus the AMPK inhibitor Compound C, respectively, and subsequently exposed to cigarette smoke to induce COPD. (A) Flow cytometry was performed to measure the percentage of Treg and Th17 cells. (B) The $CD4^+CD25^+FOXP3^+$Treg cells ratio in the colon. (C) The $CD4^+IL\text{-}17A^+$Th17 cells ratio in the colon. (D) The Th17/Treg ratio in the colon. The representative gating strategy for identifying Th17 and Treg cells is provided in **Supplementary Fig. 1A,B** . $^{***}p < 0.001$ vs. Control. $^{\#\#\#}p < 0.001$ vs. Model. $^{+++}p < 0.001$ vs. Model+AZI-50. Data are presented as mean ± SD, and were analyzed using two-way ANOVA followed by Bonferroni's post-hoc test. n = 3 technical replicates, with 3 rats per group. AZI, Azithromycin; COPD, chronic obstructive pulmonary disease.

Because of the importance of Th17/Treg balance in COPD, we evaluated the effect of AZI on Th17/Treg balance. Cumulative research reports indicate that the Th17/Treg ratio is higher in the lungs and colon of COPD rats than in control rats [24,25]. Consistently, we also observed an increase in the Th17/Treg ratio in colon tissue of COPD rats. In a previous study, AZI was reported to reduce the frequency of T cells and IL-17-producing cells in lung tissue of mice infected by bacteria [26]. In retinal inflammation, AZI can increase Treg cells and restore the effector T cells (Teff)/Treg balance, thereby contributing to disease treatment [27]. Collectively, these findings show that AZI may exert therapeutic effects against inflammation and bacterial infection by modulating Th17 and Treg cell balance. Consistent with previous research results, we found that AZI can reduce the Th17/Treg ratio in colon tissue in a concentration-dependent manner. Importantly, the positive regulatory effect of AZI on the Th17/Treg balance was effectively reversed by Compound C, indicating that AMPK signaling is integral to this immunomodulatory process. In addition to the Th17/Treg balance, we also assessed cytokine levels secreted by Th17 and Treg cells. Siddhi Jain et al. [28] reported that CS exposure leads to up-regulation of pro-inflammatory factors in the lungs of COPD rats, which is inhibited by AZI administration. Similarly, we found that CS exposure led to up-regulation of pro-inflammatory factors and down-regulation of IL-10 in the jejunum and ileum of COPD rats, and these changes were reversed by AZI administration. Together, these results indicate that AZI exerts a strong effect in maintaining colonic immune homeostasis in COPD rats.

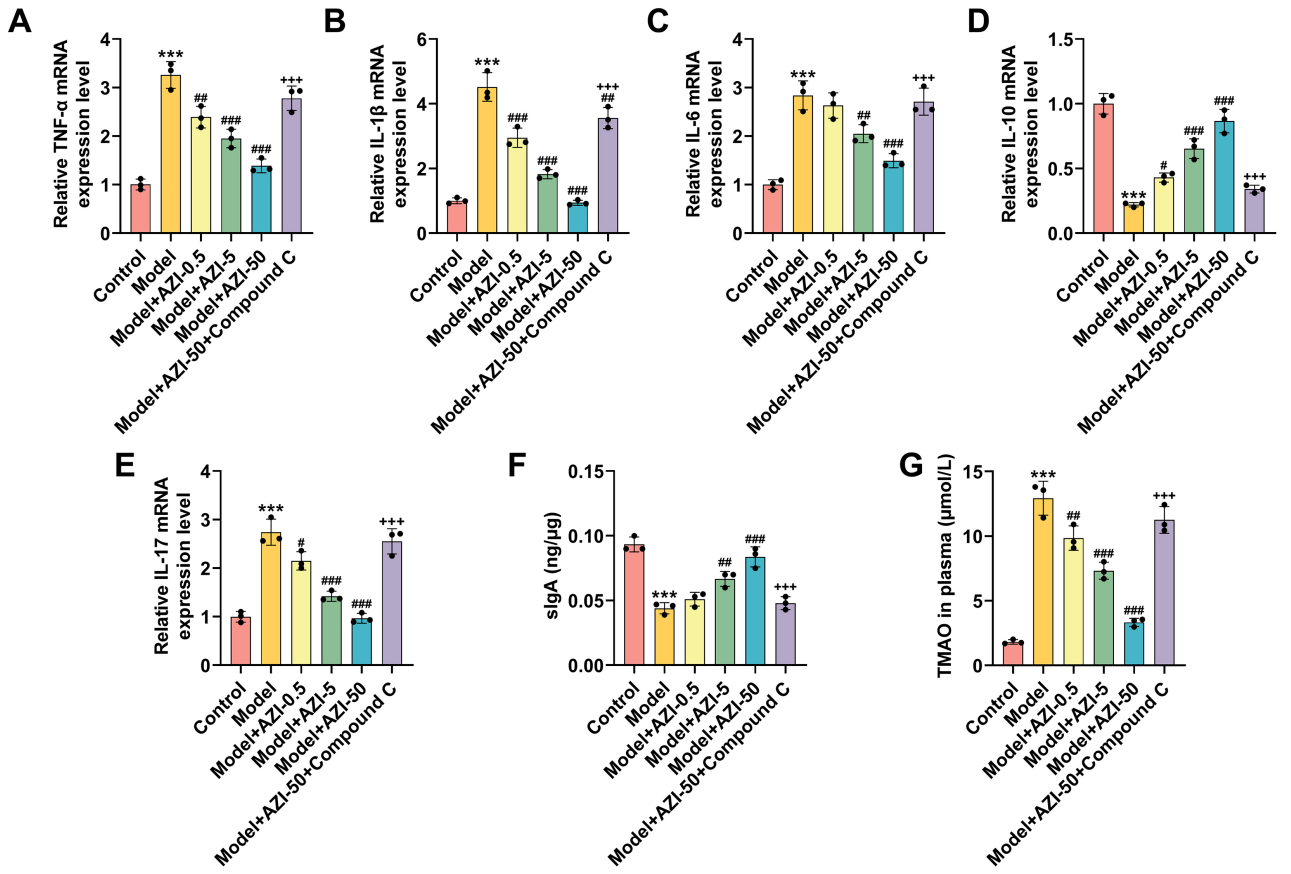

Fig. 3. Effects of AZI on the expression levels of inflammatory factors, sIgA and TMAO in COPD rats. Rats were pretreated with AZI (0.5, 5, or 50 mg/kg), or AZI (50 mg/kg) plus the AMPK inhibitor Compound C, respectively, and subsequently exposed to cigarette smoke to induce COPD. (A–E) The expression of inflammatory factors (TNF-α, IL-1β, IL-6, IL-10 and IL-17) in the jejunum and ileum was determined by qRT-PCR. GAPDH was used as the internal control. (F) The levels of sIgA in the jejunum and ileum were determined by ELISA. (G) Plasma TMAO levels were determined by liquid chromatography with triple-quadrupole mass spectrometry. $^{***}p < 0.001$ vs. Control. $^{\#}p < 0.05$, $^{\#\#}p < 0.01$, $^{\#\#\#}p < 0.001$ vs. Model. $^{+++}p < 0.001$ vs. Model+AZI-50. Data are presented as mean ± SD, and were analyzed using two-way ANOVA followed by Bonferroni's post-hoc test. n = 3 technical replicates, with 3 rats per group. AZI, Azithromycin; COPD, chronic obstructive pulmonary disease; qRT-PCR, quantitative real-time polymerase chain reaction; GAPDH, Glyceraldehyde-3-phosphate dehydrogenase; sIgA, secretory IgA; TNF-α, tumor necrosis factor-α; IL, interleukin; ELISA, Enzyme-Linked Immunosorbent Assay; TMAO, Trimethylamine N-oxide.

Intestinal mucosal immune system and intestinal microflora are two key components of the gut-lung axis; therefore, we further evaluated the effects of AZI on intestinal microflora in COPD rats. As the main mediator of intestinal mucosal immunity, sIgA plays an important role in the intestinal-pulmonary axis. In addition, a previous study found that sIgA levels in the intestinal mucosa of COPD rats were negatively correlated with the expression of harmful bacteria and harmful metabolites in intestinal microorganisms [29]. TMAO is a harmful metabolite of the intestinal microflora, and elevated circulating levels are associated with increased long-term all-cause mortality in patients with COPD [30]. In our study, AZI increased sIgA levels and decreased TMAO content simultaneously, suggesting a potential role in maintaining intestinal microflora homeostasis in COPD rats. Notably, the suppressive effect of AZI on TMAO and its promotive effect on sIgA were both compromised by AMPK inhibition, linking modulation of the gut microbial ecosystem to AMPK activation.

Furthermore, it has been reported that TMAO can promote inflammatory responses by inhibiting the AMPK/SIRT1 signaling pathway [31]. It is worth noting that the AMPK/SIRT1 pathway plays an important role in Th17/Treg cell balance [32]. AMPK functions as an upstream regulator of SIRT1, and this signaling axis has been implicated in controlling the differentiation and functions of CD4 T cell subpopulations [33]. In necrotizing enterocolitis, chronic periodontitis, and experimental autoimmune encephalomyelitis, evidence has shown that promoting SIRT1 expression can increase Treg cell

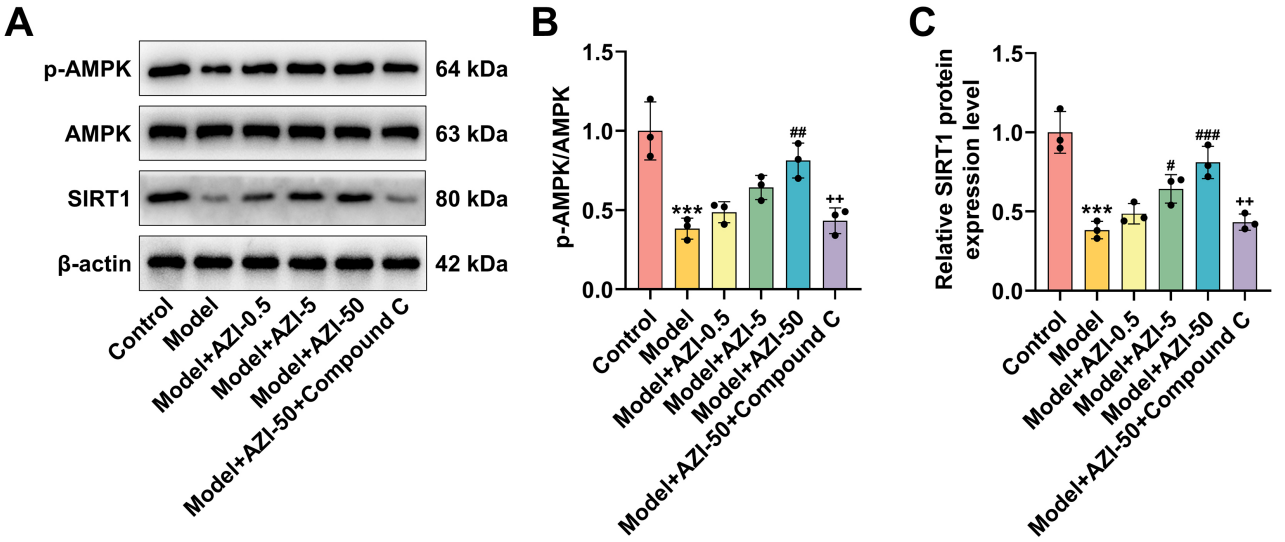

Fig. 4. Effects of AZI on the AMPK pathway and SIRT1 expression in colon tissues of COPD rats. Rats were pretreated with AZI (0.5, 5, or 50 mg/kg), or AZI (50 mg/kg) plus the AMPK inhibitor Compound C, respectively, and subsequently exposed to cigarette smoke to induce COPD. (A–C) The protein levels of AMPK pathway-related markers and SIRT1 were determined by Western blotting. β-actin was used as internal control. $^{***}p < 0.001$ vs. Control. $^{\#}p < 0.05$, $^{\#\#}p < 0.01$, $^{\#\#\#}p < 0.001$ vs. Model. $^{++}p < 0.01$ vs. Model+AZI-50. Data are presented as mean ± SD, and were analyzed using two-way ANOVA followed by Bonferroni's post-hoc test. n = 3 technical replicates, with 3 rats per group. AZI, Azithromycin; COPD, chronic obstructive pulmonary disease; SIRT1, sirtuin 1.

differentiation while inhibiting Th17 cell differentiation, thereby maintaining Th17/Treg cell balance and achieving disease relief [34,35,36]. Moreover, the study by Emad H M Hassanein et al. [37] reported that AZI may alleviate acute lung injury in rats by upregulating SIRT1. In our study, AZI activated the AMPK/SIRT1 pathway in a concentration-dependent manner, suggesting that AZI may maintain Th17/Treg cell balance through this mechanism, thereby ameliorating COPD. Our findings suggest that regulation of the AMPK/SIRT1 pathway was associated with the protective effects of AZI, as co-administration of Compound C suppressed the AMPK/SIRT1 axis and reversed the improvements in Th17/Treg balance and overall disease pathology, thereby linking AZI-induced AMPK activation to its therapeutic effects.

It should be noted that some limitations still exist in this study. First, in this study, MLI and additional structural quantitative analyses were not included to further validate the establishment of the model. Although the model was comprehensively evaluated based on histopathological alterations, inflammatory responses, and functional changes, the absence of quantitative structural assessment may limit the robustness of model validation. Then, although we demonstrated that the AMPK inhibitor Compound C reversed the protective effects of AZI, the use of a pharmacological inhibitor alone cannot fully exclude potential off-target effects. Genetic approaches, such as AMPK knockdown or knockout models, would provide more definitive evidence for the specific involvement of the AMPK/SIRT1 pathway. Furthermore, AZI is a well-known antibiotic with potentially profound and complex effects on the gut microbiota. An in-depth exploration of the microbiota's composition and function will be crucial for a comprehensive understanding of AZI's mechanisms of action in the context of COPD. We also acknowledge a limitation regarding tissue processing. In this study, jejunum and ileum tissues were analyzed as pooled samples. This approach may have obscured segment-specific differences and limited the precision of our conclusions. Future studies will analyze the jejunum and ileum separately to determine whether AIZ exerts region-specific effects.

Conclusion

In summary, our study demonstrates that AZI alleviates COPD-associated gut-lung axis dysfunction in a rat model, an effect associated with TMAO reduction, AMPK/SIRT1 activation, and subsequent restoration of Th17/Treg cell balance. These findings provide new insights into the potential of targeting the gut microbiota–mucosal immunity axis in COPD management and lay the groundwork for future studies employing genetic models to delineate the precise mechanistic contributions of the AMPK/SIRT1 pathway.

Availability of Data and Materials

The analyzed datasets generated during the study are available from the corresponding author on reasonable request.

Author Contributions

CQX and GPJ designed the research study; GHZ, JW, WGR and STJ performed the research; LJZ, LZ and YZS collected and analyzed the data. LQH made substantial contributions to the analysis and interpretation of data, and has been involved in drafting the manuscript. All authors have been involved in revising the manuscript critically for important intellectual content and gave final approval of the version to be published. All authors have participated sufficiently in the work to take public responsibility for appropriate portions of the content and agreed to be accountable for all aspects of the work in ensuring that questions related to its accuracy or integrity.

Ethics Approval and Consent to Participate

The protocol has the approval of the Ethics Committee of Zhejiang Provincial Laboratory Animal Center for Experimental Animals Welfare (ZJCLA-IACUC-20011009). The animal experiments were conducted in adherence with the ARRIVE Guidelines 2.0.

Acknowledgment

Not applicable.

Funding

This work was supported by 2023 Annual Health Science and Technology Project of Hangzhou City (Key Project) under Grant [number ZD20230011], 2022 Huzhou Science and Technology Bureau Project under Grant [number 2022GY49] and 2025 Natural Science Foundation of Zhejiang Province (Key Project) under Grant [number LHDMZ25H290003].

Conflict of Interest

The authors declare no conflict of interest.

Supplementary Material

Supplementary material associated with this article can be found, in the online version, at https://doi.org/10.24976/Discov.Med.202638211.199.

References

[1] Sandelowsky H, Weinreich UM, Aarli BB, Sundh J, Høines K, Stratelis G, et al. COPD - do the right thing. BMC Family Practice. 2021; 22: 244. https://doi.org/10.1186/s12875-021-01583-w

[2] Guo P, Li R, Piao TH, Wang CL, Wu XL, Cai HY. Pathological Mechanism and Targeted Drugs of COPD. International Journal of Chronic Obstructive Pulmonary Disease. 2022; 17: 1565–1575. https://doi.org/10.2147/COPD.S366126

[3] Qu L, Cheng Q, Wang Y, Mu H, Zhang Y. COPD and Gut-Lung Axis: How Microbiota and Host Inflammasome Influence COPD and Related Therapeutics. Frontiers in Microbiology. 2022; 13: 868086. https://doi.org/10.3389/fmicb.2022.868086

[4] Meng F, Li N, Li D, Song B, Li L. The presence of elevated circulating trimethylamine N-oxide exaggerates postoperative cognitive dysfunction in aged rats. Behavioural Brain Research. 2019; 368: 111902. https://doi.org/10.1016/j.bbr.2019.111902

[5] Liu Y, Liu Z, Tu T, Liu H, Tan C, Feng D, et al. Lycopene attenuates trimethylamine-N-oxide-induced senescence in endothelial progenitor cells via the AMPK/SIRT1 pathway. Clinical and Experimental Hypertension (New York, N.Y. : 1993). 2025; 47: 2487891. https://doi.org/10.1080/10641963.2025.2487891

[6] Heidary M, Ebrahimi Samangani A, Kargari A, Kiani Nejad A, Yashmi I, Motahar M, et al. Mechanism of action, resistance, synergism, and clinical implications of azithromycin. Journal of Clinical Laboratory Analysis. 2022; 36: e24427. https://doi.org/10.1002/jcla.24427

[7] Uzun S, Djamin RS, Kluytmans JAJW, Mulder PGH, van't Veer NE, Ermens AAM, et al. Azithromycin maintenance treatment in patients with frequent exacerbations of chronic obstructive pulmonary disease (COLUMBUS): a randomised, double-blind, placebo-controlled trial. The Lancet. Respiratory Medicine. 2014; 2: 361–368. https://doi.org/10.1016/S2213-2600(14)70019-0

[8] Peters J, Anzueto A. Azithromycin once daily for 1 year reduced acute COPD exacerbations. Annals of Internal Medicine. 2012; 156: JC1–10. https://doi.org/10.7326/0003-4819-156-2-201201170-02010

[9] Park HK, Choi Y, Lee DH, Kim S, Lee JM, Choi SW, et al. Altered gut microbiota by azithromycin attenuates airway inflammation in allergic asthma. The Journal of Allergy and Clinical Immunology. 2020; 145: 1466–1469.e8. https://doi.org/10.1016/j.jaci.2020.01.044

[10] Liu YJ, Tang B, Wang FC, Tang L, Lei YY, Luo Y, et al. Parthenolide ameliorates colon inflammation through regulating Treg/Th17 balance in a gut microbiota-dependent manner. Theranostics. 2020; 10: 5225–5241. https://doi.org/10.7150/thno.43716

[11] Lourenço JD, Ito JT, Martins MDA, Tibério IDFLC, Lopes FDTQDS. Th17/Treg Imbalance in Chronic Obstructive Pulmonary Disease: Clinical and Experimental Evidence. Frontiers in Immunology. 2021; 12: 804919. https://doi.org/10.3389/fimmu.2021.804919

[12] Wuyts WA, Willems S, Vos R, Vanaudenaerde BM, De Vleeschauwer SI, Rinaldi M, et al. Azithromycin reduces pulmonary fibrosis in a bleomycin mouse model. Experimental Lung Research. 2010; 36: 602–614. https://doi.org/10.3109/01902148.2010.492895

[13] Jia Y, He T, Wu D, Tong J, Zhu J, Li Z, et al. The treatment of Qibai Pingfei Capsule on chronic obstructive pulmonary disease may be mediated by Th17/Treg balance and gut-lung axis microbiota. Journal of Translational Medicine. 2022; 20: 281. https://doi.org/10.1186/s12967-022-03481-w

[14] Li X, Jamal M, Guo P, Jin Z, Zheng F, Song X, et al. Irisin alleviates pulmonary epithelial barrier dysfunction in sepsis-induced acute lung injury via activation of AMPK/SIRT1 pathways. Biomedicine & Pharmacotherapy = Biomedecine & Pharmacotherapie. 2019; 118: 109363. https://doi.org/10.1016/j.biopha.2019.109363

[15] Zhang F, Guo F, Liu Y, Zhang Y, Li D, Yang H. Shema Oral Liquid Ameliorates the Severity of LPS-Induced COPD *via* Regulating DNMT1. Frontiers in Pharmacology. 2022; 13: 903593. https://doi.org/10.3389/fphar.2022.903593

[16] Wang J, Ren C, Jin L, Batu W. Seabuckthorn Wuwei Pulvis attenuates chronic obstructive pulmonary disease in rat through gut microbiota-short chain fatty acids axis. Journal

of Ethnopharmacology. 2023; 314: 116591. https://doi.org/10.1016/j.jep.2023.116591

[17] Li J, Xie Y, Zhao P, Qin Y, Oliver BG, Tian Y, et al. A chinese herbal formula ameliorates COPD by inhibiting the inflammatory response via downregulation of p65, JNK, and p38. Phytomedicine : International Journal of Phytotherapy and Phytopharmacology. 2021; 83: 153475. https://doi.org/10.1016/j.phymed.2021.153475

[18] Li J, Zeng Q, Xiong Z, Xian G, Liu Z, Zhan Q, et al. Trimethylamine N-oxide induces osteogenic responses in human aortic valve interstitial cells in vitro and aggravates aortic valve lesions in mice. Cardiovascular Research. 2022; 118: 2018–2030. https://doi.org/10.1093/cvr/cvab243

[19] Liu XY, Su JC, Zhang XF, Xiang SY, Yi CM, Wang YW, et al. Electroacupuncture preconditioning improves pulmonary function via inhibiting inflammatory response and up-regulating expression of ACE2 and Ang (1-7) in lipopolysaccharide-induced acute lung injury rats. Zhen ci yan jiu = Acupuncture Research. 2022; 47: 684–689. (In Chinese)

[20] Guan P, Cai WT, Jiang F, Li W, Zeng M, Wu J. Caveolin-1 improves lung injury in rats with chronic obstructive pulmonary disease partially through Wnt/β-catenin signaling pathway. Journal of Biological Regulators and Homeostatic Agents. 2020; 34: 457–465. https://doi.org/10.23812/20-71-A-37

[21] Wan YF, Huang ZH, Jing K, Li J, Wang Y, Xu CQ, et al. Azithromycin attenuates pulmonary inflammation and emphysema in smoking-induced COPD model in rats. Respiratory Care. 2015; 60: 128–134. https://doi.org/10.4187/respcare.03344

[22] Elkholy SE, Maher SA, Abd El-Hamid NR, Elsayed HA, Hassan WA, Abdelmaogood AKK, et al. The immunomodulatory effects of probiotics and azithromycin in dextran sodium sulfate-induced ulcerative colitis in rats via TLR4-NF-κB and p38-MAPK pathway. Biomedicine & Pharmacotherapy = Biomedecine & Pharmacotherapie. 2023; 165: 115005. https://doi.org/10.1016/j.biopha.2023.115005

[23] Stellari FF, Sala A, Donofrio G, Ruscitti F, Caruso P, Topini TM, et al. Azithromycin inhibits nuclear factor-κB activation during lung inflammation: an in vivo imaging study. Pharmacology Research & Perspectives. 2014; 2: e00058. https://doi.org/10.1002/prp2.58

[24] Wang Y, Li N, Li Q, Liu Z, Li Y, Kong J, et al. Xuanbai Chengqi Decoction Ameliorates Pulmonary Inflammation via Reshaping Gut Microbiota and Rectifying Th17/Treg Imbalance in a Murine Model of Chronic Obstructive Pulmonary Disease. International Journal of Chronic Obstructive Pulmonary Disease. 2021; 16: 3317–3335. https://doi.org/10.2147/COPD.S337181

[25] Zhang X, Li X, Ma W, Liu F, Huang P, Wei L, et al. Astragaloside IV restores Th17/Treg balance via inhibiting CXCR4 to improve chronic obstructive pulmonary disease. Immunopharmacology and Immunotoxicology. 2023; 45: 682–691. https://doi.org/10.1080/08923973.2023.2228479

[26] Borkner L, Misiak A, Wilk MM, Mills KHG. Azithromycin Clears *Bordetella pertussis* Infection in Mice but Also Modulates Innate and Adaptive Immune Responses and T Cell Memory. Frontiers in Immunology. 2018; 9: 1764. https://doi.org/10.3389/fimmu.2018.01764

[27] Huang J, Li Z, Hu Y, Chen G, Li Z, Xie Y, et al. Azithromycin modulates Teff/Treg balance in retinal inflammation via the mTOR signaling pathway. Biochemical Pharmacology. 2021; 193: 114793. https://doi.org/10.1016/j.bcp.2021.114793

[28] Jain S, Durugkar S, Saha P, Gokhale SB, Naidu VGM, Sharma P. Effects of intranasal azithromycin on features of cigarette smoke-induced lung inflammation. European Journal of Pharmacology. 2022; 915: 174467. https://doi.org/10.1016/j.ejphar.2021.174467

[29] Mao J, Li Y, Bian Q, Xuan Y, Li J, Wang Z, et al. The Bufei Jianpi Formula Improves Mucosal Immune Function by Remodeling Gut Microbiota Through the SCFAs/GPR43/NLRP3 Pathway in Chronic Obstructive Pulmonary Disease Rats. International Journal of Chronic Obstructive Pulmonary Disease. 2022; 17: 1285–1298. https://doi.org/10.2147/COPD.S359428

[30] Ottiger M, Nickler M, Steuer C, Bernasconi L, Huber A, Christ-Crain M, et al. Gut, microbiota-dependent trimethylamine-N-oxide is associated with long-term all-cause mortality in patients with exacerbated chronic obstructive pulmonary disease. Nutrition (Burbank, Los Angeles County, Calif.). 2018; 45: 135–141.e1. https://doi.org/10.1016/j.nut.2017.07.001

[31] Zhou S, Xue J, Shan J, Hong Y, Zhu W, Nie Z, et al. Gut-Flora-Dependent Metabolite Trimethylamine-N-Oxide Promotes Atherosclerosis-Associated Inflammation Responses by Indirect ROS Stimulation and Signaling Involving AMPK and SIRT1. Nutrients. 2022; 14: 3338. https://doi.org/10.3390/nu14163338

[32] Ma F, Hao H, Gao X, Cai Y, Zhou J, Liang P, et al. Melatonin ameliorates necrotizing enterocolitis by preventing Th17/Treg imbalance through activation of the AMPK/SIRT1 pathway. Theranostics. 2020; 10: 7730–7746. https://doi.org/10.7150/thno.45862

[33] Ellmeier W, Seiser C. Histone deacetylase function in $CD4^+$ T cells. Nature Reviews. Immunology. 2018; 18: 617–634. https://doi.org/10.1038/s41577-018-0037-z

[34] Gao X, Liu W, Gao P, Li S, Chen Z, Ma F. Melatonin-induced lncRNA LINC01512 prevents Treg/Th17 imbalance by promoting SIRT1 expression in necrotizing enterocolitis. International Immunopharmacology. 2021; 96: 107787. https://doi.org/10.1016/j.intimp.2021.107787

[35] Zheng Y, Dong C, Yang J, Jin Y, Zheng W, Zhou Q, et al. Exosomal microRNA-155-5p from PDLSCs regulated Th17/Treg balance by targeting sirtuin-1 in chronic periodontitis. Journal of Cellular Physiology. 2019; 234: 20662–20674. https://doi.org/10.1002/jcp.28671

[36] Wang J, Zhao C, Kong P, Bian G, Sun Z, Sun Y, et al. Methylene blue alleviates experimental autoimmune encephalomyelitis by modulating AMPK/SIRT1 signaling pathway and Th17/Treg immune response. Journal of Neuroimmunology. 2016; 299: 45–52. https://doi.org/10.1016/j.jneuroim.2016.08.014

[37] Hassanein EHM, Sayed GA, Alzoghaibi AM, Alammar AS, Abdel-Wahab BA, Abd El-Ghafar OAM, et al. Azithromycin Mitigates Cisplatin-Induced Lung Oxidative Stress, Inflammation and Necroptosis by Upregulating SIRT1, PPARγ, and Nrf2/HO-1 Signaling. Pharmaceuticals (Basel, Switzerland). 2022; 16: 52. https://doi.org/10.3390/ph16010052